Structural Distortion of the TpCo-L Fragment (Tp = tris(pyrazolyl)borate). Analysis by X-ray Diffraction and Density Functional Theory

Jennifer L. Detrich, Robert Konečný, William M. Vetter, Douglas Doren,*,† Arnold L. Rheingold, and Klaus H. Theopold*,‡

Contribution from the Department of Chemistry and Biochemistry, Center for Catalytic Science and Technology, University of Delaware, Newark, Delaware 19716

Received July 13, 1995[⊗]

Abstract: The crystal structures of coordinatively unsaturated [$(Tp^{Np}Co)_2(\mu\text{-}N_2)$] and $Tp^{Np}Co(CO)$ show "bent" molecules, in which the fourth ligand (N_2, CO) is bent away from the pseudo-threefold axis of the TpCo-moiety by 27−38°. Magnesium reduction of $Tp^{t\text{-}Bu,Me}Co(CO)$ yielded $[Tp^{t\text{-}Bu,Me}Co(\mu\text{-}CO)]_2Mg(THF)_4$ which was also structurally characterized; the reduced carbonyl is "linear". Extended Hückel theory (EHT) and density functional theory (DFT) have been used to analyze the electronic structures and structural preferences of the TpCo-L fragment with L = CO (Co^I, d^8), COLi (Co^0, d^9), and I (Co^{II}, d^7). The actual and theoretical structure determinations were in good agreement. Based on these results we suggest that d^8 TpCo-L complexes and, by analogy, isoelectronic CpM-L complexes assume "bent" structures.

Introduction

During our investigation of dioxygen activation by cobalt complexes we have prepared and structurally characterized several complexes of the type TpCo-L,[1,2] where Tp is a sterically hindered tris(pyrazolyl)borate ligand[3] of the so-called "tetrahedral enforcer" variety,[4] and L is a two-electron donor (e.g., N_2, CO, C_2H_4). These four-coordinate Co(I) complexes are two electrons short of the commonly expected 18 valence electron configuration, and they exhibit paramagnetism due to the two unpaired electrons of a triplet ground state. While one might intuitively have expected a "linear" structure for molecules of this type (see **A** in Chart 1, i.e., L on or close to the line connecting the B and Co atoms, point group C_{3v}), they actually adopt a severely "bent" geometry (see **B**, point group C_s).

We were especially intrigued by this structural choice, and its possible ramifications for reactivity, because the TpCo-L moiety is isoelectronic with, and chemically related to Cp*M-L (Cp* = η^5-C_5Me_5, M = Rh, Ir, L = PR_3, CO), a generic fragment having gained much notoriety during the past decade for its indiscriminate addition of unactivated C−H bonds of alkanes.[5−11] Indeed, it has been shown that Tp*M-L (Tp* = hydrotris(3,5-dimethylpyrazolyl)borate, M = Rh, Ir) accomplishes the same feat.[12,13] Due to their unprecedented reactivity, the structures of these unstable intermediates have been both of great interest and hard to determine. The cobalt complexes described herein may thus serve as closely related, yet stable, models for the more reactive rhodium and iridium analogs.

Chart 1

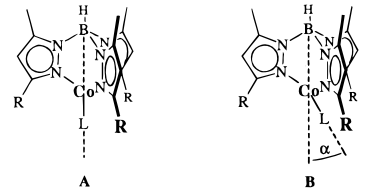

The structure of coordination compounds of transition metals depends strongly on the formal oxidation state (i.e., the number of d-electrons, d^n) of the central metal. Bearing in mind the obvious connection between structure and reactivity, and ever searching for means of controlling the latter, we were curious how changes in oxidation state might impact the structure of the TpCo-L fragment. Accordingly, we also report the structure of a reduction product of such a complex, namely $[Tp^{t\text{-}Bu,Me}Co(\mu\text{-}CO)]_2Mg(THF)_4$ ($Tp^{t\text{-}Bu,Me}$ = hydrotris(3-*tert*-butyl-5-methylpyrazolyl)borate). This compound is nearly linear, as are previously reported Co(II) complexes of the type TpCo-X. It would appear that the bent geometry (**B**) for TpCo-L complexes is unique to the d^8 electron configuration.

To understand the structural choices of the system, we turned to theory. While the gross structural features (i.e., "bent" versus "linear") were predicted even by simple EHMO (extended Hückel molecular orbital) calculations, we have also been able to calculate remarkably accurate molecular structures using density functional theory (DFT). We offer these results as proof that computational technology has now advanced to the point where predicted geometries of complicated inorganic molecules are in excellent agreement with (and in some ways better than) those determined experimentally. These findings provide much encouragement for our plans to use DFT calculations for the characterization of more ephemeral molecules, such as reaction

† E-mail: doren@udel.edu.
‡ E-mail: theopold@strauss.udel.edu.
⊗ Abstract published in *Advance ACS Abstracts,* February 1, 1996.

(1) Egan, J. W., Jr.; Haggerty, B. S.; Rheingold, A. L.; Sendlinger, S. C.; Theopold, K. H. *J. Am. Chem. Soc.* **1990**, *112*, 2445.
(2) Reinaud, O. M.; Theopold, K. H. *J. Am. Chem. Soc.* **1994**, *116*, 6979.
(3) Trofimenko, S. *Chem. Rev.* **1993**, *93*, 943.
(4) Trofimenko, S.; Calabrese, J. C.; Thompson, J. S. *Inorg. Chem.* **1987**, *26*, 1507.
(5) Janowicz, A. H.; Bergman, R. G. *J. Am. Chem. Soc.* **1982**, *104*, 352.
(6) Hoyano, J. K.; Graham, W. A. G. *J. Am. Chem. Soc.* **1982**, *104*, 3723.
(7) Hoyano, J. K.; McMaster, A. D.; Graham, W. A. G. *J. Am. Chem. Soc.* **1983**, *105*, 7190.
(8) Janowicz, A. H.; Bergman, R. G. *J. Am. Chem. Soc.* **1983**, *105*, 3929.
(9) Jones, W. D.; Feher, F. J. *J. Am. Chem. Soc.* **1984**, *106*, 1650.
(10) Bergman, R. G. *Science* **1984**, *223*, 902.
(11) Jones, W. D.; Feher, F. J. *Acc. Chem. Res.* **1989**, *22*, 91.
(12) Jones, W. D.; Hessell, E. T. *J. Am. Chem. Soc.* **1993**, *115*, 554.
(13) (a) Ghosh, C. K.; Graham, W. A. G. *J. Am. Chem. Soc.* **1987**, *109*, 4727. (b) Ghosh, C. K.; Graham, W. A. G. *J. Am. Chem. Soc.* **1989**, *111*, 375.

0002-7863/96/1518-1703$12.00/0

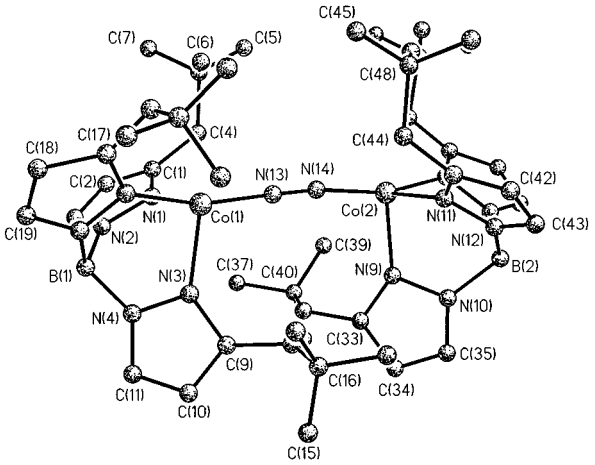

Figure 1. The molecular structure of $[(Tp^{Np}Co)_2(\mu\text{-}N_2)]$. Selected interatomic distances and angles are listed in Table 1.

intermediates and transition states of transition metal catalyzed reactions. It should be noted, that the d^8 CpM-L fragment (M = Co, Rh, Ir) has been the subject of several theoretical studies, including both EHT and DFT calculations.[14,15] The apparent parallels in the electronic structures of TpCo-L and CpCo-L lend credence to our suggestion that the former are good chemical models for the latter.

Results and Discussion

Syntheses and Structures. The structure determination of $Tp^{t\text{-}Bu,Me}Co(O_2)$ ($Tp^{t\text{-}Bu,Me}$ = hydrotris(3-*tert*-butyl-5-methylpyrazolyl)borate), which revealed the first example of a side-on bound superoxide ligand,[1] led us to ponder the possibility that other diatomic ligands coordinated to the $Tp^{t\text{-}Bu,Me}Co$-moiety might also exhibit unusual bonding modes. However, much to our frustration, neither $Tp^{t\text{-}Bu,Me}Co(N_2)$ nor $Tp^{t\text{-}Bu,Me}Co(CO)$ yielded crystals suitable for a diffraction study, and the crystal structure determinations of their analogs $Tp^{t\text{-}Bu}Co(N_2)$ and $Tp^{t\text{-}Bu}Co(CO)$ ($Tp^{t\text{-}Bu}$ = hydrotris(3-*tert*-butylpyrazolyl)borate) were marred by positional disorder of the diatomic ligands about a crystallographic mirror plane, thereby obstructing the view of the relevant parts of the molecules. Inspired by the absence of similar mirror symmetry in a molecule containing the newly prepared Tp^{Np}-ligand,[16] we finally decided to prepare $Tp^{Np}Co$-L (Tp^{Np} = hydrotris(3-neopentylpyrazolyl)borate; L = N_2, CO), in hopes of settling the structural question. As before, magnesium reduction of the halide precursor $Tp^{Np}CoI$ under a nitrogen atmosphere resulted in a color change from blue to brown within ca. 30 min. Subsequent workup and recrystallization from pentane gave brown crystals of dinuclear $[(Tp^{Np}Co)_2(\mu\text{-}N_2)]$ in reasonable yield (64%). Its infrared spectrum provided the first evidence for a difference in the binding mode of the dinitrogen ligand; the N−N stretching vibration (ν_{N-N}: 2056 cm^{-1}) appeared much less intense and was shifted to slightly higher frequency compared to those of mononuclear $Tp^{t\text{-}Bu,Me}Co(N_2)$ (ν_{N-N}: 2046 cm^{-1})[1] and $Tp^{t\text{-}Bu}Co(N_2)$ (ν_{N-N}: 2046 cm^{-1}).

The result of an X-ray crystal structure determination of $[(Tp^{Np}Co)_2(\mu\text{-}N_2)]$ is shown in Figure 1, and selected interatomic distances and angles are listed in Table 1. The molecule is a dinuclear coordination compound and exhibits no crystallographically imposed symmetry. The two cobalt fragments are linked by a bridging dinitrogen ligand which is bound in an end-on fashion to both metal centers; the short N−N distance of 1.14(3) Å is consistent with a description as a Co(I) complex of neutral dinitrogen (N−N, 1.0975 Å), rather than a hydrazido (N_2^{4-}) ligand as encountered for example in $[(C_5Me_5)Me_3W]_2(\mu\text{-}N_2)$ (N−N, 1.334(26) Å)[17,18] and $[(dme)Cl_2(Ph_2C_2)W]_2(\mu\text{-}N_2)$ (N−N, 1.292(16) Å).[19] Indeed, all the structural parameters associated with the dinitrogen coordination (Co(1)−N(13), 1.774(22) Å; Co(2)−N(14), 1.847(21) Å; Co(1)−N(13)−N(14), 175.7(21)°; Co(2)−N(14)−N(13), 171.7(18)°) fall within the range established by other cobalt complexes of this molecule.[20−22] Regarding the Tp^{Np}-ligand also, the relevant distances (Co−N_{av}, 2.032 Å) and angles (N−Co−N_{av}, 91.6°) are not unusual for this class of tripod ligands.[3,16] However, the molecule features one unusual structural detail. Rather than sitting on the pseudo-threefold axes of the metal fragments (defined by the B−Co vectors), the N_2-ligand is bent away from the former by large angles α (see Chart 1, α(1) = 34.7°, α(2) = 37.8°). This distortion of the pseudotetrahedral CoN_4-units takes the molecule most of the way toward two linked "cis-divacant octahedra" (i.e., an octahedron from which two ligands cis to each other have been removed; α for this structure is 54.7°). Of course, in an isolated case such a distortion might be attributed to steric interactions between the bulky ligands of the dinuclear complex or to crystal packing forces, rather than reflecting the inherent preference of the metal atom.

Table 1. Selected Interatomic Distances and Angles for $[Tp^{Np}Co]_2(\mu\text{-}N_2)$ (**1**)

Distances (Å)			
Co(1)−N(1)	2.057(20)	Co(2)−N(7)	2.025(20)
Co(1)−N(3)	2.012(25)	Co(2)−N(9)	2.027(23)
Co(1)−N(5)	2.006(22)	Co(2)−N(11)	2.065(20)
Co(1)−N(13)	1.774(22)	Co(2)−N(14)	1.847(21)
N(13)−N(14)	1.141(30)		
Angles (deg)			
N(1)−Co(1)−N(3)	92.2(9)	N(7)−Co(2)−N(11)	92.7(9)
N(1)−Co(1)−N(5)	91.2(8)	N(7)−Co(2)−N(9)	89.1(8)
N(3)−Co(1)−N(5)	90.1(9)	N(9)−Co(2)−N(11)	93.4(9)
Co(1)−N(13)−N(14)	175.7(21)	Co(2)−N(14)−N(13)	171.7(18)
B(1)−Co(1)−N(13)	145.3	B(1)−Co(2)−N(14)	142.1

Exposure of a pentane solution of said $[Tp^{Np}Co]_2(\mu\text{-}N_2)$ to an excess of CO resulted in an immediate color change to green. Removal of solvent and recrystallization from pentane afforded blue-green crystals of $Tp^{Np}Co(CO)$ in near quantitative yield. Its IR spectrum showed ν_{CO} at 1950 cm^{-1} and curiously weak for a metal carbonyl (i.e., the band is less intense than the C−H stretches of the molecule). For comparison, CpCo(CO) has been generated transiently in solution by low temperature photolysis, and its CO stretch was reported at 1993−1999 cm^{-1}, depending on the solvent.[23] The molecular structure of $Tp^{Np}Co(CO)$ is depicted in Figure 2, and selected interatomic distances and angles are compiled in Table 2. As expected, the carbonyl complex is mononuclear, with a terminal CO-ligand. There is not crystallographic symmetry in the molecule, and the CO ligand shows no sign of disorder. The metric parameters of the carbonyl ligation (C(1)−O, 1.145(6) Å; Co−C(1), 1.769-

(14) Hofmann, P.; Padmanabhan, M. *Organometallics* **1983**, *2*, 1273.
(15) Ziegler, T.; Tschinke, V.; Fan, L.; Becke, A. D. *J. Am. Chem. Soc.* **1989**, *111*, 9177.
(16) Calabrese, J. C.; Trofimenko, S. *Inorg. Chem.* **1992**, *31*, 4810.
(17) Murray, R. C.; Schrock, R. R. *J. Am. Chem. Soc.* **1985**, *107*, 4557.
(18) O'Regan, M. B.; Liu, A. H.; Finch, W. C.; Schrock, R. R.; Davis, W. M. *J. Am. Chem. Soc.* **1990**, *112*, 4331.
(19) Churchill, M. R.; Li, Y.-J.; Theopold, K. H.; Schrock, R. R. *Inorg. Chem.* **1984**, *23*, 4472.
(20) Davis, B. R.; Payne, N. C.; Ibers, J. A. *Inorg. Chem.* **1969**, *8*, 2719.
(21) Jones, R. A.; Stuart, A. L.; Atwood, J. L.; Hunter, W. E. *Organometallics* **1983**, *2*, 1437.
(22) Cecconi, F.; Ghilardi, C. A.; Midollini, S.; Moneti, S.; Orlandini, A.; Bacci, M. *J. Chem. Soc., Chem. Comm.* **1985**, 731.
(23) (a) Dougherty, T. P.; Heilweil, E. J. *J. Chem. Phys.* **1994**, *100*, 4006. (b) Bengali, A. A.; Bergman, R. G.; Moore, C. B. *J. Am. Chem. Soc.* **1995**, *117*, 3879.

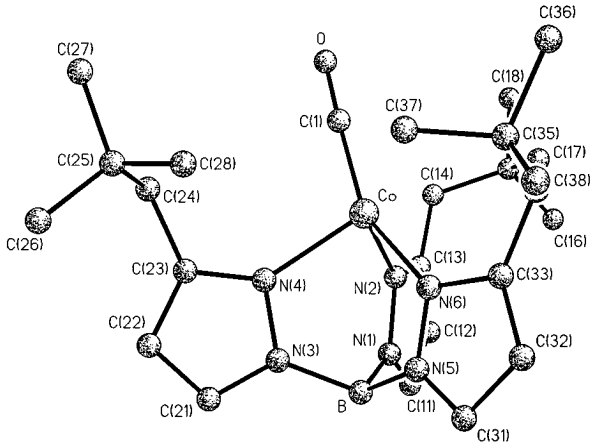

Figure 2. The molecular structure of $Tp^{Np}Co(CO)$. Selected interatomic distances and angles are listed in Table 2.

Table 2. Selected Interatomic Distances and Angles for $Tp^{Np}Co(CO)$ (**2**)

Distances (Å)			
Co−N(2)	2.055(5)	Co−N(4)	2.055(4)
Co−N(6)	2.010(4)	Co−C(1)	1.769(5)
C(1)−O	1.145(6)		
Angles (deg)			
N(2)−Co−N(4)	93.2(2)	N(4)−Co−N(6)	91.1(2)
N(2)−Co−N(6)	90.6(2)	Co−C(1)−O	177.8(6)
B−Co−C(1)	153.4		

(5) Å; Co−C(1)−O, 177.8(6)°) are entirely unexceptional,[24] as are those of the Tp^{Np}-coordination (Co−N_{av}, 2.040 Å, N−Co−N_{av}, 91.6°). However, once again, the diatomic ligand (CO) is bent away from the pseudo-threefold axis by $\alpha = 26.6°$, thus putting it approximately trans to N(6). $Tp^{Np}Co(CO)$ is a mononuclear complex, and the carbonyl is effectively screened from intermolecular contacts by the wall of neopentyl groups. It suffers no close contacts to neighboring molecules. Given the similarity in the direction and extent (α) of the distortion, the latter appears to be intrinsic to this class of compounds.

The structures described above are in fact not isolated examples. All complexes of the type TpCo-L, where L is a neutral two-electron ligand, exhibit the same distortion. Other examples prepared and structurally characterized in our laboratory include $[Tp^{i\text{-}Pr,Me}Co]_2(\mu\text{-}N_2)$ with $\alpha = 25.9°$ ($Tp^{i\text{-}Pr,Me}$ = hydrotris(3-isopropyl-5-methylpyrazolyl)borate) and $Tp^{t\text{-}Bu,Me}$-$Co(C_2H_4)$ with $\alpha = 25.7°$.[25] Furthermore, the disorder in the crystal structures of $Tp^{t\text{-}Bu}Co(N_2)$ and $Tp^{t\text{-}Bu}Co(CO)$ is now easily interpreted as averaging of inherently distorted molecules by a crystallographic mirror plane. Considering the similarity between the Tp- and Cp-ligands and concurring with theoretical considerations,[14,15] unsaturated CpCo-L fragments are probably "bent" as well. The same may well be true of the heavier congeners containing rhodium and iridium. However, these species are distinguished from CpCoL by their extreme affinity for ligands of all kinds (including noble gases!),[26−28] which may render irrelevant the notion of true 16-electron complexes (i.e., CpRhL, CpIrL) in any chemically interesting environment.

All commonly used models for rationalizing and predicting structures of transition metal compounds place heavy emphasis upon the d-electron count. Having found a particular coordination geometry for the d^8 configuration of Co(I), we wondered how either removal or addition of electrons might change the structural preference of the TpCo-L moiety. From an experimental standpoint, this meant preparing analogous complexes in other oxidation states. Accordingly, magnesium reduction of $Tp^{t\text{-}Bu,Me}Co(CO)$ in THF yielded a dark reddish-purple solution, from which the reduced carbonyl $[Tp^{t\text{-}Bu,Me}Co(\mu\text{-}CO)]_2Mg(THF)_4$ could be isolated in high yield. The result of its crystal structure determination is shown in Figure 3, and the relevant interatomic distances and angles are listed in Table 3. The molecule includes a linear chain of three metal atoms, consisting of two $Tp^{t\text{-}Bu,Me}Co$-moieties at either end and one central magnesium ion. The chain is linked by two isocarbonyl ligands, i.e., CO molecules bound to metal ions both at their carbon (Co) and oxygen (Mg) termini. This bonding mode is well precedented, and the present example exhibits the typical symptoms of such coordination.[29,30] Thus, the shortened metal carbon bonds (Co−C_{av}, 1.69 Å) and significant lengthening of the carbon−oxygen bond (C−O_{av}, 1.228 Å) are consistent with strong backbonding from an extremely electron rich Co(0) atom and a Co═C═O|→Mg^{2+} resonance structure. The extremely low C−O stretching frequency of $\nu_{CO} = 1642\ cm^{-1}$ is also in agreement with this picture. The lower oxidation state of the cobalt is reflected in the relatively longer bonds to nitrogen (Co−N_{av}, 2.177 Å), which are accompanied by a slight reduction in the ligand bite angle (N−Co−N_{av}, 88.2°). The approximate linearity of the whole array (Co−C−O_{av}, 177°; C−O−Mg_{av}, 127°; O−Mg−O, 178°) is slightly unusual, but can probably be attributed to steric factors. For the purpose of this study, however, the most important feature of the structure is the lack

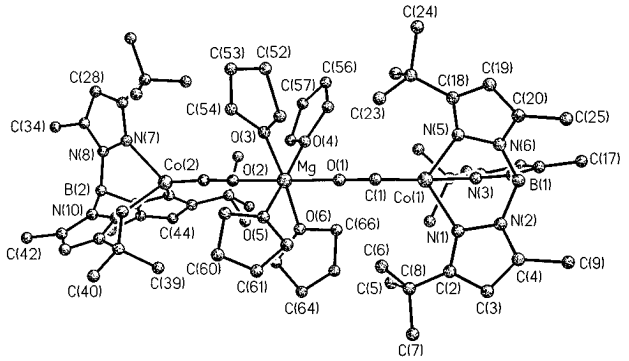

Figure 3. The molecular structure of $[Tp^{t\text{-}Bu,Me}Co(\mu\text{-}CO)]_2Mg(THF)_4$. Selected interatomic distances and angles are listed in Table 3.

Table 3. Selected Interatomic Distances and Angles for $(Tp'CoCO)_2Mg(THF)_4$ (**3**)

Distances (Å)			
Co(1)−N(1)	2.190(2)	Co(2)−N(7)	2.193(2)
Co(1)−N(3)	2.221(2)	Co(2)−N(9)	2.192(2)
Co(1)−N(5)	2.152(2)	Co(2)−N(11)	2.165(2)
Co(1)−C(1)	1.701(2)	Co(2)−C(26)	1.679(2)
C(1)−O(1)	1.225(2)	C(26)−O(2)	1.231(2)
Mg−O(1)	2.063(1)	Mg−O(2)	2.072(1)
Angles (deg)			
N(1)−Co(1)−N(3)	85.8(7)	N(7)−Co(2)−N(11)	85.7(6)
N(1)−Co(1)−N(5)	90.5(7)	N(7)−Co(2)−N(9)	85.5(7)
N(3)−Co(1)−N(5)	87.3(7)	N(9)−Co(2)−N(11)	94.6(7)
Co(1)−C(1)−O(1)	177.5(15)	Co(2)−C(26)−O(2)	176.8(19)
C(1)−O(1)−Mg	167.1(14)	C(26)−O(2)−Mg	175.8(14)
B(1)−Co(1)−C(1)	176.4	B(2)−Co(2)−C(26)	176.4

(24) Orpen, A. G.; Brammer, L.; Allen, F. H.; Kennard, O.; Watson, D. G. *J. Chem. Soc., Dalton Trans.* **1989**, S1.
(25) Reinaud, O. M.; Detrich, J. L.; Theopold, K. H., unpublished results.
(26) Weiller, B. H.; Wasserman, E. P.; Bergman, R. G.; Moore, C. B.; Pimentel, G. C. *J. Am. Chem. Soc.* **1989**, *111*, 8288.
(27) Bengali, A. A.; Schultz, R. H.; Moore, C. B.; Bergman, R. G. *J. Am. Chem. Soc.* **1994**, *116*, 9585.
(28) Partridge, M. G.; McCamley, A.; Perutz, R. N. *J. Chem. Soc., Dalton Trans.* **1994**, 3519.
(29) Horwitz, C. P.; Shriver, D. F. *Adv. Organomet. Chem.* **1984**, *23*, 219.
(30) Vrtis, R. N.; Bott, S. G.; Lippard, S. J. *Organometallics* **1992**, *11*, 270 and references therein.

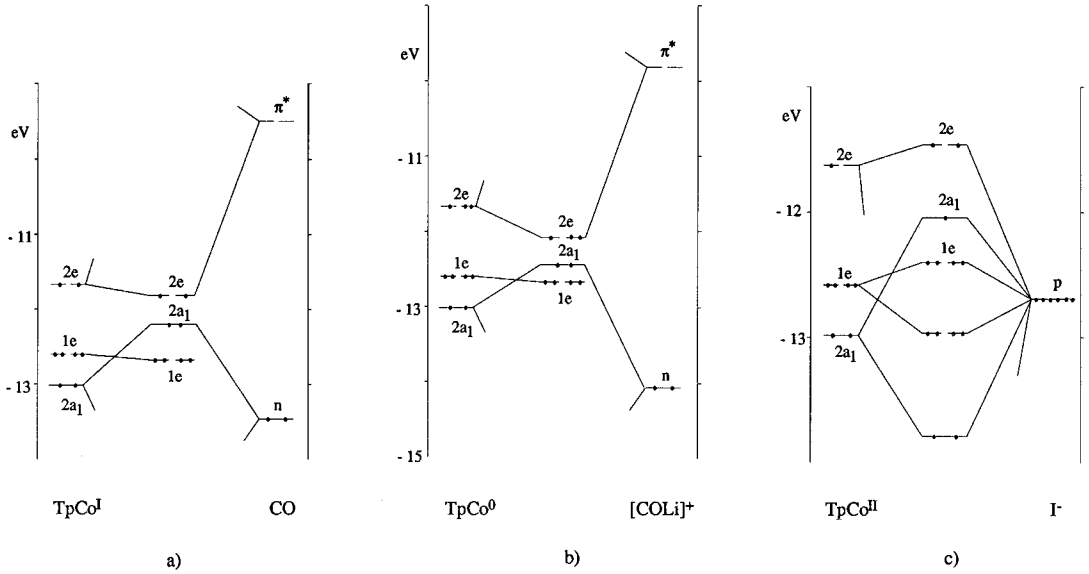

Figure 4. Schematic EHT interaction diagram of TpCoL in the linear configuration: (a) L = CO, (b) L = $[COLi]^+$, and (c) L = I^-. Only the important MOs of TpCoL and the contributing fragment orbitals are shown.

of any significant distortion from a linear (**A**-type) structure, i.e., $\alpha = 3.6°$. We conclude that the TpCo-L fragment with a d^9 electron count shows no tendency to distort to a bent **B**-type structure.

Finally, we consider TpCo-L complexes containing Co(II) (d^7). From our own work, there is $Tp^{i\text{-}Pr,Me}CoI$, which has the iodide ligand situated squarely on the pseudo-threefold axis of the complex ($\alpha = 3.3°$)[31] and $Tp^{t\text{-}Bu}CoMe$ with $\alpha = 2.8°$.[25] We are not aware of any TpCo-complexes in which CO or N_2 are bound to Co(II), but several examples of complexes with unsaturated anionic ligands (such as NCS^-, NCO^-, N_3^-) are known. Where such complexes have been crystallographically characterized, their structures were found to be of type **A**, showing no significant deviation from C_{3v} symmetry.[4,16]

These findings suggest that there is something special about TpCo-L complexes with a d^8 electron count, which forces such compounds to distort from the intuitively preferred structure, namely a trigonally distorted tetrahedron (**A**), toward a cis-divacant octahedron. The effect is sharply delineated, as it does not appear to operate on compounds with d^7 or d^9 configurations. It may extend to chemically related systems, such as CpM-L (M = Co, Rh, Ir), and the high reactivity of these fragments is probably related to the "openness" of the metal atom.

Theory and Calculations. To gain insight into the electronic structure of TpCo-L, extended Hückel theory (EHT) and density functional theory (DFT) calculations were carried out for a set of complexes with different ligands L (L = CO, COLi, and I). These ligands differ in their respective σ- and π-bonding capabilities, and they are associated with different electron occupations of the metal's valence orbitals (i.e., different formal oxidation states of Co). We will show that each of these factors play key roles in determining the geometry of TpCo-L. Details of the calculations are described in the Theoretical Methods Section. While the steric bulk of the tris(pyrazolyl)borate ligands is presumably responsible for the chemical stability of coordinatively unsaturated 16-electron TpCo-L complexes, the detailed structures of these complexes appear insensitive to the nature of the alkyl substitutents in the 3-position of the pyrazole rings. The electronic effects of the substituents were judged minor, and therefore we have used unsubstituted tris(pyrazolyl)-borate (abbreviated Tp, i.e., $[HB(C_3H_3N_2)_3]^-$) for all calculations. This alteration significantly reduces computational time. Even the unsubstituted Tp-ligand is unusually large for current first principles calculations. The efficiency of the DFT method makes it possible to include electron correlation in this large molecule at a reasonable computational expense. First principles theory of coordination compounds (including those containing Tp-ligands)[32] has typically been limited to much smaller model compounds, which must be artificially constrained to maintain the pseudo tetrahedral environment around the metal center. These additional approximations are not necessary with the DFT method, and it permits the prediction of geometries and relative energies of different geometries, rather than simply analyzing the electronic structure and energy of a given geometry.

The qualitative aspects of bonding in these compounds can be understood by fragment analysis. The TpCo fragment has C_{3v} symmetry; its N−Co−N angles are diminished from the ideal tetrahedral value by approximately 14°. This pyramidal distortion and the presence of a fourth, chemically different ligand, change the energy level ordering of the four-coordinate complexes from that expected in T_d symmetry. The relative energies of the MOs of TpCo-L are determined by the σ- and π-bonding between L and the Co atom, and thus change with the angle α.

First we consider the prototypical π-acceptor, CO. The interactions between the frontier orbitals of the TpCo fragment and CO are shown for the linear geometry (C_{3v} symmetry) in Figure 4a; not unexpectedly, the diagram is closely analogous to that of CpCo(CO).[14] Both EHT and DFT calculations show that the main interactions are σ-mixing of the $2a_1$ orbital of TpCo with a carbon-based lone pair of CO (n) and back-donation from the metal 2e SOMOs of TpCo to π^* on CO. There is only a weak interaction of the 1e orbitals of TpCo with the π^* orbitals of CO in C_{3v} symmetry. Thus, the net effect of the interaction of the TpCo fragment with a π-acceptor and σ-donor is to move the $2a_1$ orbital energetically closer to the 2e orbitals. Note, that the $^3A_2$ electronic ground state in the C_{3v} geometry is not degenerate, so that the observed distortion cannot be attributed to a first-order Jahn-Teller effect. It will be seen that changes in the energy of the $2a_1$ and the 2e MOs upon bending of the Co−CO bond determine whether the bond is bent or linear.

(31) Reinaud, O. M.; Rheingold, A. L.; Theopold, K. H. *Inorg. Chem.* **1994**, *33*, 2306.

(32) Ruggiero, C. E.; Carrier, S. M.; Antholine, W. E.; Whittaker, J. W.; Cramer, C. J.; Tolman, W. B. *J. Am. Chem. Soc.* **1993**, *155*, 11285.

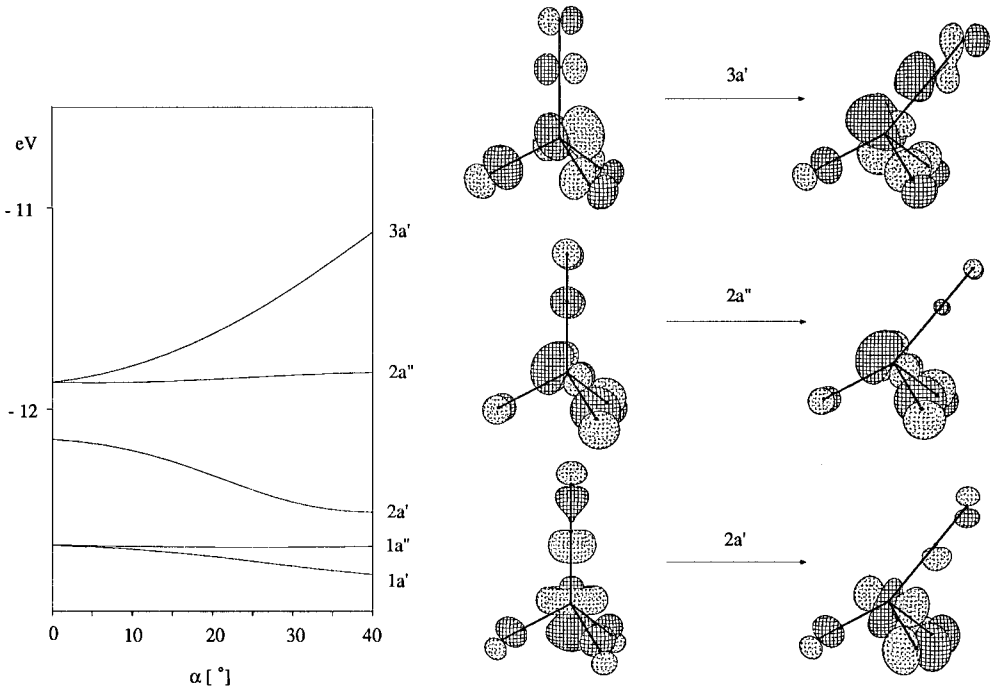

Figure 5. EHT Walsh diagram for TpCo(CO) as CO is bent away from the threefold axis. (Most significant metal orbital contributions to EHT molecular orbitals in linear geometry [2a′, 65% d_{z^2}; 2a″, 37% d_{xy}, 9% d_{yz}; 3a′, 37% $d_{x^2-y^2}$, 9% d_{xz}] and in bent geometry ($\alpha = 40°$) [2a′, 25% $d_{x^2-y^2}$, 10% d_{z^2}, 10% d_{xz}; 2a″ 37% d_{xy}, 15% d_{yz}; 3a′ 25% d_{xz}, 12% $d_{x^2-y^2}$, 8% d_{z^2}]). The 1e orbitals are not shown because EHT predicts negligible contributions from the CO ligand to these orbitals. However, see Figure 10 for illustration of these orbitals as predicted by DFT.

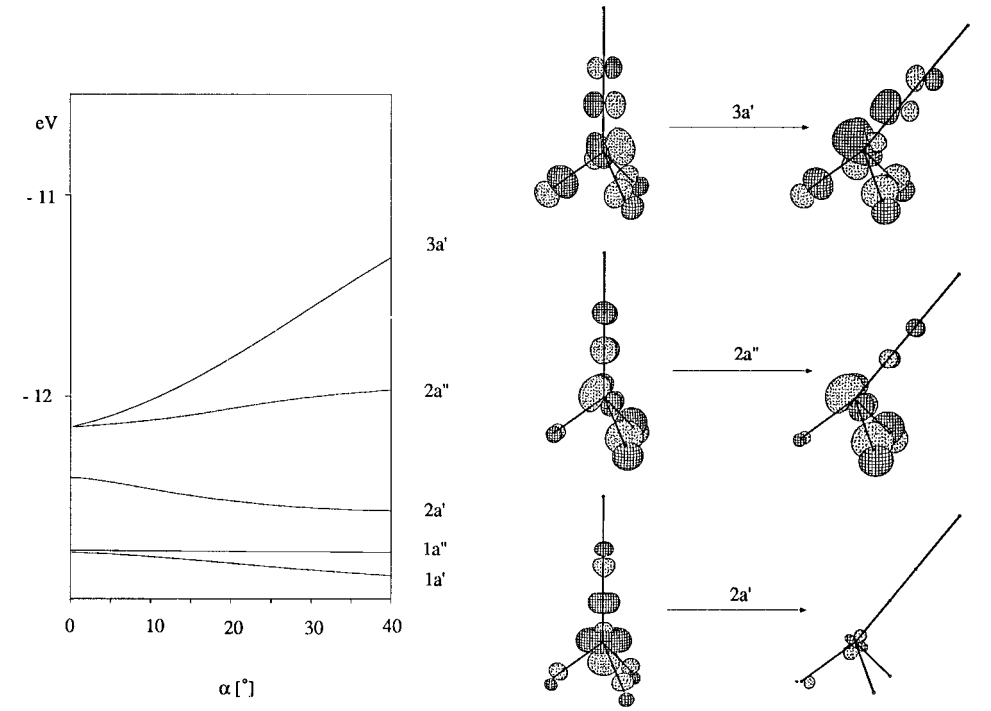

Figure 6. EHT Walsh diagram for TpCo(μ-CO)Li as $[COLi]^+$ is bent away from the threefold axis. (Most significant metal orbital contributions to EHT molecular orbitals in linear geometry [2a′, 75% d_{z^2}; 2a″, 27% d_{xy}, 13% d_{yz}; 3a′, 25% $d_{x^2-y^2}$, 12% d_{xz}] and in bent geometry ($\alpha = 40°$) [2a′, 5% $d_{x^2-y^2}$, 1% d_{z^2}, 1% d_{xz}; 2a″, 28% d_{xy}, 22% d_{yz}; 3a′, 33% d_{xz}, 9% $d_{x^2-y^2}$, 6% d_{z^2}]). The 1e orbitals are not shown because EHT predicts negligible contributions from the $[COLi]^+$ ligand to these orbitals.

We have used EHT calculations to generate Walsh diagrams to analyze the electronic and geometric features of TpCo-L molecules. Although extended Hückel theory has well-known weaknesses, our EHT analyses (using the X-ray determined structures for the TpCo fragments and Co-L bond lengths) are in good qualitative agreement with the more reliable DFT calculations. Figure 5 depicts a Walsh diagram for TpCo(CO), showing the effect of bending the carbonyl ligand away from the C_3 axis. This reduces the symmetry to C_s. Both e sets (1e, 2e) split as the bending angle α deviates from 0°. The total energy of the system (Figure 8a) decreases upon bending, primarily because the doubly occupied 2a′ level is stabilized by mixing with the singly occupied 3a′ level. The metal contribution to the 2a′ orbital is mostly d_{z^2} at $\alpha = 0°$. Bending CO away from the threefold axis reduces the antibonding d_{z^2}-n(CO) interaction and permits a favorable metal$-\pi^*$(CO) interaction. As the angle increases, the character of the 2a′ orbital changes from d_{z^2} to a mixture of $d_{x^2-y^2}$, d_{z^2} and d_{xz}. This

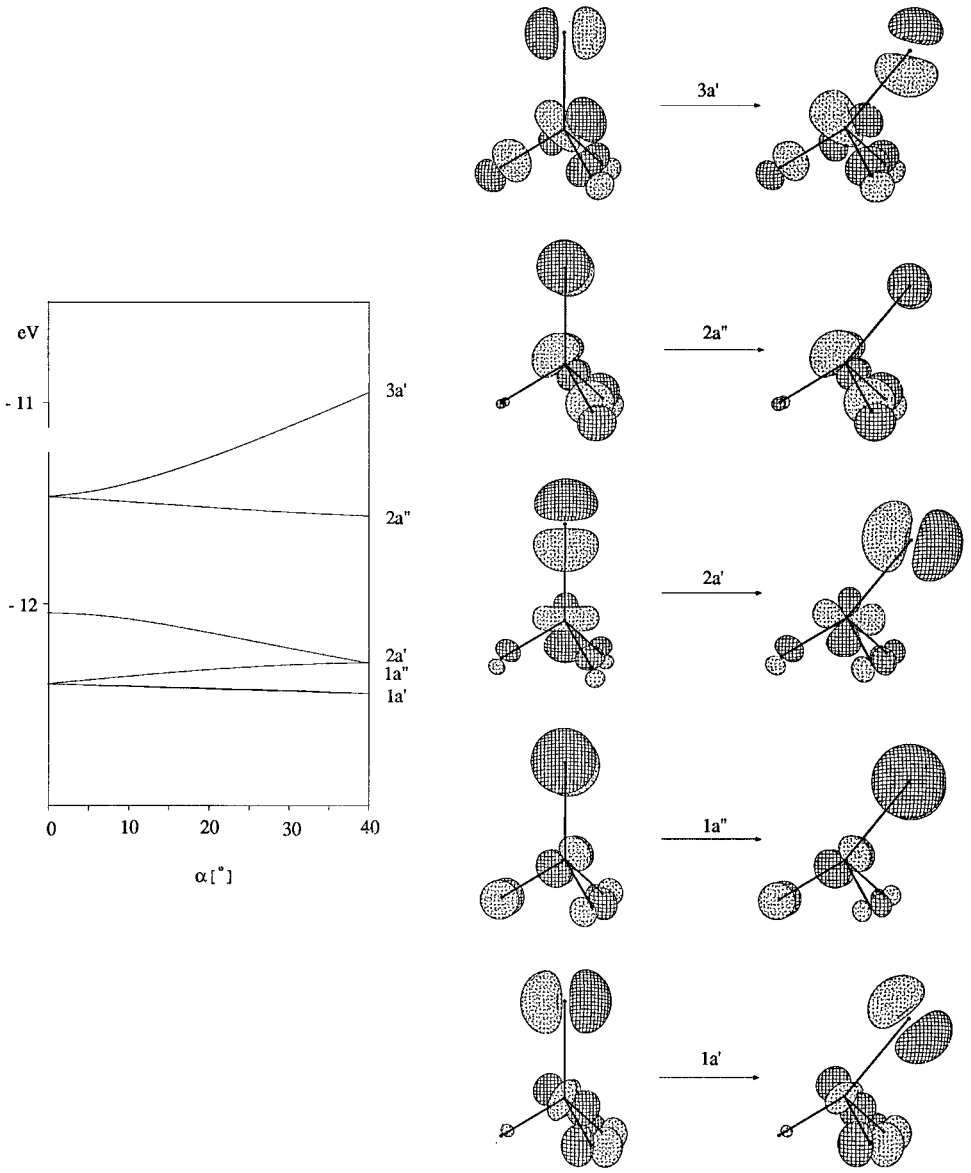

Figure 7. EHT Walsh diagram for TpCoI as I is bent away from the threefold axis. (Most significant metal orbital contributions to EHT molecular orbitals in linear geometry [1a′, 24% $d_{x^2-y^2}$, 12% d_{xz}; 1a″, 24% d_{xy}, 12% d_{yz}; 2a′, 51% d_{z^2}] and in bent geometry ($\alpha = 40°$) [1a′, 17% $d_{x^2-y^2}$, 10% d_{xz}, 3% d_{z^2}; 1a″, 26% d_{xy}, 10% d_{yz}; 2a′, 29% d_{z^2}, 10% $d_{x^2-y^2}$, 3% d_{xz}]).

mixing, which is not compatible with C_{3v} symmetry, enhances the metal−π* interaction. On the other hand, the singly occupied 3a′ level is destabilized by this mixing, weakening the metal−π*(CO) interaction. The increase in 3a′ energy opposes bending of the carbonyl. Thus, the mixing of the 2a′ and 3a′ orbitals that is permitted in C_s symmetry accounts for the observed bent structure. This is a second-order Jahn-Teller effect, although it differs from the typical textbook examples in that the dominant mixing involves occupied orbitals, and not the LUMO.[33]

Parity prevents the 2a″ level from mixing with the a′ levels in C_s symmetry. Bending causes reduced overlap between the metal and π*(CO) in the 2a″ level, causing reduced backbonding and slight destabilization of this MO. In contrast to the energy changes for the 2e and $2a_1$ levels, the total gain in energy due to orbital energy variations of the 1e levels is insignificant. The 1a′ level is somewhat destabilized by π*(CO) components; the energy of the 1a″ level does not change.

(33) Albright, T. A.; Burdett, J. K.; Whangbo, M. H. *Orbital Interactions in Chemistry*; Wiley: New York: 1985; pp 95−98.

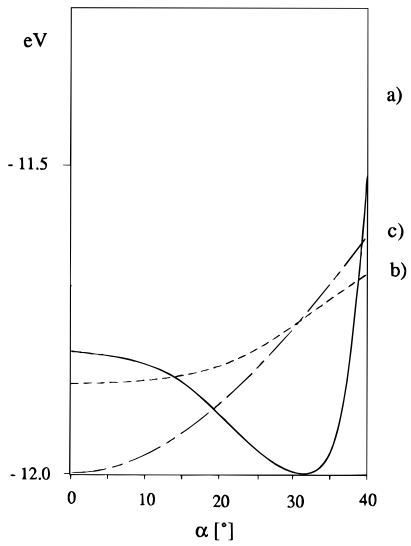

Figure 8. EHT total energy as a function of bending angle, α: (a) TpCo(CO) (—), (b) TpCo(μ-CO)Li (— —), and (c) TpCoI (- — - —).

The ground state of TpCo(CO) is a triplet, as found experimentally, and as predicted by DFT. Although the 2e level is split by bending of CO, the resulting energy gap between the 3a′ and 2a″ orbitals is smaller (0.31 eV as calculated by EHT) than the pairing energy of the two valence electrons, so these two levels will be singly occupied. The total electronic energy for the triplet state has its minimum at $\alpha > 0$ (see Figure 8a). Thus, EHT predicts a bent geometry, although the predicted angle ($\alpha = 32°$) is not quantitatively correct.

Quantitative predictions of geometry and energy can be made with DFT. Coordinates from the crystal structure determination of $Tp^{Np}Co(CO)$ were used as the starting point for the DFT calculation. Hydrogen atom positions are not well determined by X-ray diffraction, and accordingly the bonds to hydrogen were unreasonably short. DFT calculations with atomic positions from the X-ray structure predict large forces on atoms bonded to hydrogen, and the unrealistic structure makes it difficult to obtain a converged wave function. When the CO coordinates were optimized with all other atoms fixed at their positions from the X-ray structure, the bending angle was significantly underestimated. Therefore a full geometry optimization including all atoms was performed.

Calculations were carried out with two different DFT approximations to the exchange-correlation potential: the local spin density approximation (LSD) and the Becke-Perdew nonlocal spin density approximation (NLSD). The LSD and NLSD calculations were done with the programs DMol[34] and DGauss,[35] respectively. The main technical difference is that DMol uses basis functions that are given numerically on an atom-centered, spherical-polar mesh, while DGauss employs Gaussian basis functions. In the minimum energy structure for TpCoCO predicted with LSD, α is 32.9°. Calculations at the LSD level for the linear geometry of TpCoCO, with α fixed at 0°, in C_{3v} symmetry, predict that the "linear" geometry is less stable by 9 kcal/mol. Table 4 shows the predicted bond lengths, bond angles, and energies of calculated geometries and compares them with the experimental structures. The geometry of TpCo(CO) predicted with NLSD is closer to the experimental geometry than the LSD results, but the two theories gave qualitatively similar results. The angle α in TpCo(CO) was predicted by NLSD to be 27.7°, compared to the experimental value of 26.6°. The linear geometry is less stable by 8 kcal/mol at the NLSD level of theory. Converged positions of all other heavy atoms using both LSD and NLSD agree with the X-ray structure of 0.03 Å (0.11 Å in the case of the Co−N distances from LSD). The predicted bond lengths to H-atom are longer than those derived from X-ray diffraction by 0.13 Å for the C−H bonds and by 0.09 Å for the B−H bond. This result is expected, and the theoretical values for H-atom positions are believed to be more accurate than the X-ray values.

The energies of the most important NLSD frontier orbitals of TpCo(CO) in the optimal geometry are shown in Figure 9a, and the orbital shapes are depicted in Figure 10. The qualitative description of the energies and orbitals are similar to those from EHT. Due to the low symmetry of the molecule (C_s point group), the composition and ordering of the frontier orbitals are complex. The Co contribution to the two doubly occupied orbitals, 1a′ and 1a″,[36] is primarily d_{yz} with a smaller d_{xy} component.[37] Both are stabilized by interactions with the π^* orbitals on CO, though these interactions are stronger in the 1a′ orbital. At somewhat higher energy is the doubly occupied 2a′ orbital, which is primarily a mixture of d_{z^2}, $d_{x^2-y^2}$, and d_{xz} metal orbitals. Figure 10 shows no significant metal−n(CO) antibonding interaction in this orbital. At highest energy are two singly occupied orbitals (SOMO's), 2a″ and 3a′, which are mixtures primarily of d_{xy} and d_{yz} and of d_{xz}, $d_{x^2-y^2}$, and d_{z^2}, respectively. These orbitals clearly show the metal−π^*(CO) interaction. The 2a′ orbital energy in the optimal bent geometry is 0.28 eV lower than in the linear geometry, while the 3a′ orbital energy is higher by 0.07 eV.

Table 4. Comparison of Structural Parameters Obtained by DFT Calculations and X-ray Diffraction

	TpCo(CO)				
	LSD		NLSD		$Tp^{Np}Co(CO)$
	linear	bent	linear	bent	X-ray
Co−C [Å]	1.76	1.74	1.85	1.79	1.77
C−O [Å]	1.17	1.17	1.17	1.18	1.15
Co−N [Å]	1.90	1.93	1.99	2.02	2.04
α [deg]	0	33.2	0	27.7	26.6
Co−C−O [deg]	180	177.9	180	176.0	177.8
N−Co−N [deg]	92.0	92.5	90.6	90.9	91.2
ΔE [kcal/mol]	9.01		7.96		

	TpCo(μ-COLi) LSD	$[Tp^{t\text{-}Bu,Me}Co(CO)]_2Mg(THF)_4$ X-ray
Co−C [Å]	1.66	1.69
C−O [Å]	1.24	1.23
O−M [Å][a]	1.65	2.07
Co−N [Å]	1.95	2.18
α [deg]	3.4	3.6
Co−C−O [deg]	178.5	177.9
C−O−M [deg]	177.7	171.5
N−Co−N [deg]	90.8	88.2

	TpCoI				
	LSD		NLSD		$Tp^{iPr,Me}CoI$
	doublet	quartet	doublet	quartet	X-ray
Co−I [Å]	2.43	2.45	2.52	2.53	2.54
Co−N [Å]	1.88	1.96	1.95	2.02	2.02
α [deg]	4.9	4.7	10.4	3.8	3.3
N−Co−N [deg]	91.6	92.1	91.0	94.1	94.0

[a] The difference between these values is partly due to the different metals in the theoretical model compound (M = Li) and the molecule as synthesized (M = Mg).

We have also calculated vibrational frequencies for TpCo(CO). The calculated CO stretching frequency is 1967 cm^{-1}, compared to 1950 cm^{-1} found experimentally for $Tp^{Np}Co(CO)$ (0.9% difference). The calculations predict that this absorption should have the characteristic high intensity of a CO stretch, which is in contrast to the experimental observation. Measured spectra on related molecules ($Tp^{t\text{-}Bu,Me}Co(CO)$, $Tp^{t\text{-}Bu}Co(CO)$, $Tp^{Np}Co(CO)$, $Tp^{i\text{-}Pr,Me}Co(CO)$) show some dependence of the frequency and intensity of this CO stretch on substitution in the Tp rings. While the frequency difference is consistent with the lack of alkyl substituents in the computational model, the reasons for the discrepancy in the vibrational intensities are unclear.

To understand the linear structure of $[Tp^{t\text{-}Bu,Me}Co(\mu\text{-}CO)]_2Mg(THF)_4$, we have used TpCo($\mu$-CO)Li as a model for our calculations. The $[COLi]^+$ ligand is a better π-acceptor and weaker σ-donor than neutral CO, and it increases the number

(34) Delley, B. *J. Chem. Phys.* **1990**, *92*, 508.
(35) Andzelm, J.; Wimmer, E. *J. Chem. Phys.* **1992**, *96*, 1280.
(36) The orbital labels follow the usual convention for symmetry labels, except that the numbering is arbitrarily begun with the lowest energy state shown. This allows us to use the same labels for DFT and EHT orbitals. The orbital labels indicate the d orbitals that make the large contributions. This does not mean that orbitals are entirely localized on the metal.
(37) Co d-orbitals contributions at the optimal geometry from NLSD: 1a′, 31% d_{yz}, 12% d_{xy}, 2% d_{z^2}; 1a″, 7% d_{yz}, 2% d_{xy}; 2a′ 46% d_{z^2}, 17% $d_{x^2-y^2}$, 16% d_{xz}; 2a″, 43% d_{xy}, 19% d_{yx}, 1% d_{xz}; 3a′, 29% d_{xz}, 16% $d_{x^2-y^2}$, 13% d_{z^2}, 4% d_{xy}.

Table 5. Crystallographic Data for $[Tp^{Np}Co)_2(\mu\text{-}N_2)]$ (**1**), $Tp^{Np}Co(CO)$ (**2**), and $[Tp^{t\text{-}Bu,Me}Co(\mu\text{-}CO)]_2Mg(THF)_4$ (**3**)

	1	**2**	**3**
		(a) Crystal Parameters	
formula	$C_{48}H_{80}B_2Co_2N_{14}$	$C_{25}H_{52}BCoN_6O$	$C_{66}H_{112}B_2Co_2MgN_{12}O_2$
formula weight	992.7	522.5	1269.5
crystal system	monoclinic	triclinic	monoclinic
space group	$P2_1/n$	$P\bar{1}$	$P2_1/c$
a, Å	14.869(4)	11.502(3)	17.238(6)
b, Å	19.776(5)	11.589(3)	23.135(13)
c, Å	19.384(5)	12.344(3)	20.749(8)
α, deg		69.770(2)	
β, deg	91.20(3)	69.950(2)	104.12(3)
γ, deg		89.369(2)	
V, Å^3		1439.4(7)	8024(6)
Z	4	2	4
crystal dimens, mm	0.35 × 0.40 × 0.40	0.76 × 0.76 × 0.80	0.36 × 0.41 × 0.50
crystal color	brown	green	dark red
D(calc), g cm^{-3}	1.157	1.205	1.051
μ(Mo K$_\alpha$), cm^{-1}	6.25	6.23	2.67
		(b) Data Collection	
diffractometer	Siemens P4	Siemens R3	Siemens P4
monochromator	graphite	graphite	graphite
radiation	Mo K$_\alpha$	Mo K$_\alpha$	Mo K$_\alpha$
T, K	296	296	296
2*θ* scan range, deg	4−48	4−52	4−42
data collected (*h*, *k*, *l*)	−17 to +16, 0 to +21, 0 to +20	−13 to +14, −13 to +14, 0 to 15	±18, +24, +21
reflections collected	7692	5934	6190
indep. reflcns	7438	5656	4725
obsd ref ($F_o > n\sigma(F_o)$)	1948, $n = 4$	3863, $n = 4$	3269, $n = 5$
std. rflcns	3 std/197 rflcns	3 std/197 rflcns	3 std/197 rflcns
var. in stds, %	<1%	<1%	2%
		(c) Refinement	
R(*F*), %	11.05	6.60	11.16
R(*wF*), %	10.30	8.73	11.27
Δ/*σ*(max)	0.014	0.299	0.62
Δ(*ϱ*), e Å^{-3}	0.83	0.36	0.24
N_o/N_v	7.1	13.1	7.1
GOF	1.58	1.57	2.32

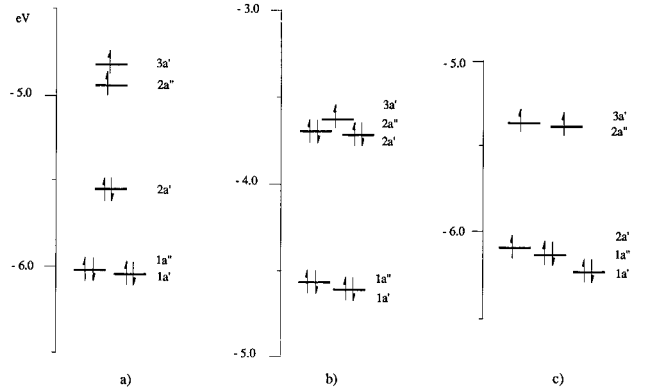

Figure 9. DFT energies of α frontier molecular orbitals in optimal geometries: (a) TpCo(CO), (b) TpCo(*μ*-CO)Li, and (c) TpCoI. Spin unrestricted calculations give different absolute energies for α ("up") and *β* ("down") spin orbitals, due to the different number of electrons in each spin state. The energies shown are for the α spin orbitals, though the occupations for both spin states are indicated. Energies for TpCoCO and TpCoI are taken from NLSD calculations. Those for TpCo(*μ*-CO)Li are from LSD calculations, and their absolute values should not be quanitatively compared to the others.

of d-electrons by one, from d^8 to d^9. In the linear configuration, the frontier orbitals of the complex are qualitatively the same as those of TpCo(CO) (see Figure 4b). The ground state of linear TpCo(*μ*-CO)Li is degenerate, and distortion from C_{3v} to C_s symmetry is consistent with a first-order Jahn-Teller effect. However, the Walsh diagram (see Figure 6) shows that the 2a″ level is not stabilized by bending, contrary to expectation for a first-order Jahn-Teller distortion. In fact, the orbital energies in TpCo(*μ*-CO)Li are determined primarily by the same second-order effects and ligand interactions that determine the structure of TpCo(CO). The Walsh diagrams for the two molecules differ only in their quantitative details. Upon bending, the added electron in the 2e level of TpCo(*μ*-CO)Li leads to stronger destabilization of the 3a′ orbital and the 2a″ orbital (which is now occupied by two electrons), with Walsh diagram slopes steeper than for TpCo(CO). The stabilization of 2a′ is not as strong as in TpCo(CO)—where it provides the driving force for bending—and it is overwhelmed by destabilization of the 2e levels. These changes are consequences of the fact that $[C{=}O|{\rightarrow}Li]^+$ is a better *π*-accepting and weaker *σ*-donating ligand than CO: stronger back-donation to *π** orbitals in the linear configuration leads to more destabilization of the 3a′ and 2a″ levels upon bending because of a bigger loss of back-bonding. On the other hand, weaker *σ*-donation leads to less stabilization of 2a′ upon bending due to weaker metal−n(CO) antibonding interaction. The net result of these two factors is to favor linearity for the d^9 species (Figure 8b).

A full geometry optimization of TpCo(*μ*-CO)Li was performed with LSD. The equilibrium structure is essentially "linear", and the metric parameters are close to the experimental values of the real compound (see Table 4). The predicted α of TpCo(*μ*-CO)Li is 3.4°, as compared to 3.6° measured for $[Tp'Co(\mu\text{-}CO)]_2Mg(THF)_4$. The calculated frontier orbital energy levels of TpCo(*μ*-CO)Li are shown schematically in Figure 9b. There is a nearly degenerate set of three high lying orbitals (3a′, 2a″, and 2a′) occupied by five electrons.

We have also performed a full geometry optimization of TpCo(*μ*-CO)Li at the NLSD level. With the nonlocal correc-

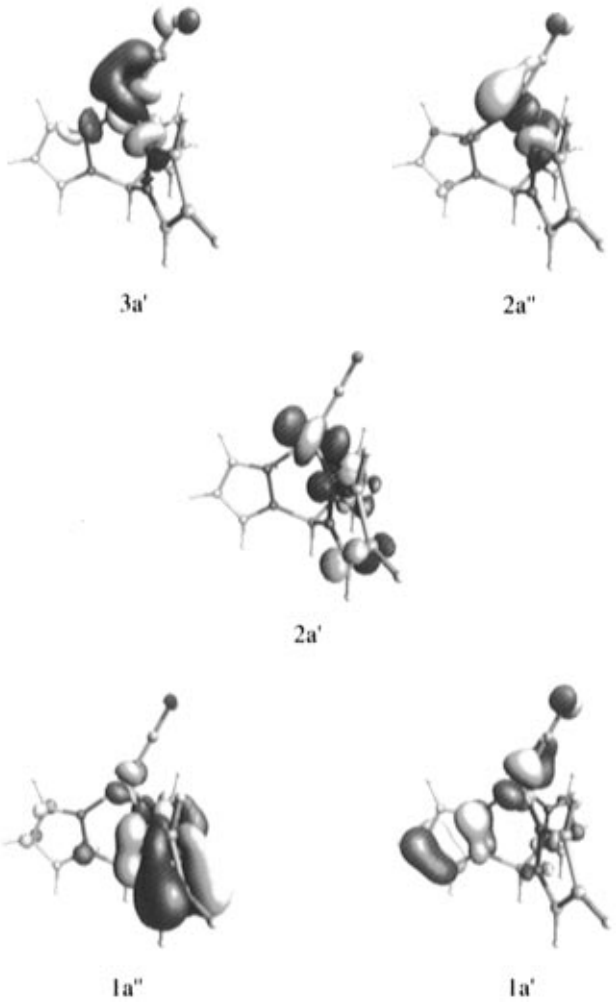

Figure 10. Pictorial representations of the frontier molecular orbitals of TpCo(CO) from the NLSD calculation at the optimal geometry.

tions, the model complex is not stable in vacuo. The O−Li bond was broken during optimization, the Li traveled to a free space between two pyrazole rings. The rest of the molecule adopted the geometry of TpCo(CO) with $\alpha = 28.6°$ and bond distances Co−Li, 2.46 Å, and C(carbonyl)−Li, 2.41 Å.

In searching for a better model at the NLSD level of theory we have performed a full geometry optimization of the $[TpCo(CO)]^-$ anion. Adding one extra electron to TpCo(CO) decreased the angle α from 27.7° (in neutral TpCo(CO)) to 19.7° (in the anion), though the bent geometry is more stable than the linear geometry by only 3.4 kcal/mol. Thus, the lower oxidation state (d^9-configuration) of $[Tp^{t\text{-}Bu,Me}Co(\mu\text{-}CO)]_2Mg(THF)_4$ by itself is not likely to account for the observed linear geometry. The σ-donating and π-accepting properties of the ligand also play a role, as noted above for COLi.

Finally, the interaction of a π-donor (e.g., L = I) with the TpCo fragment yields a somewhat different ordering of the MO levels. Figure 4c shows the result of an EHT calculation (C_{3v} symmetry). Both the 2e and $2a_1$ orbitals interact with the three low-lying degenerate filled *p*-orbitals of I. Now there is a larger energy separation between the doubly occupied 2e set and the $2a_1$ orbital. Consequently, upon bending, the $2a_1$ (2a′ in C_s symmetry) orbital is stabilized to a much smaller extent (Figure 7) than in the previous examples. The σ-antibonding interaction with the 2a′ orbital is reduced as before, but now there is also an unfavorable π-antibonding interaction. The 1a″ level is destabilized upon bending by antibonding interactions with π-donor levels of I. The 1a′ level is slightly stabilized and the 3a′ orbital is destabilized as in TpCo(CO). The measured magnetic moment of $Tp^{i\text{-}Pr,Me}CoI$ is consistent with a quartet ground state, suggesting that the 2a′, 2a″, and 3a′ orbitals are each singly occupied. In this configuration, the energetic gain upon bending due to stabilization of the 2a′ and 2a″ levels is canceled by destabilization of the 1a″ and 3a′ levels. TpCoI is predicted to be linear (Figure 8c).

A full geometry optimization, beginning with the coordinates from the crystal structure determination of $Tp^{i\text{-}Pr,Me}CoI$,[31] was performed with LSD and NLSD. The LSD calculation predicts the doublet configuration $(1a'')^2(1a')^2(2a')^2(2a'')^1$ to be more stable than the quartet $(1a'')^2(1a')^2(2a')^1(2a'')^1(3a')^1$, which is not consistent with the measured magnetic moment. The difficulties of DFT as a one-electron model in describing multiplet structures are well-known.[38,39] The energy differences between doublet and quartet states calculated with LSD is only 1.5 kcal/mol; small errors in the exchange and correlation functionals can account for this failure. The NLSD performs better, the linear quartet spin state being lower in energy by 23.1 kcal/mol than the linear doublet. However, the linear doublet state is degenerate and, as expected from a first-order Jahn-Teller effect, the doublet relaxes by bending to an angle $\alpha = 10.4°$. The bend doublet has essentially the same energy as the linear quartet, the quartet being lower by only 0.02 kcal/mol. The model used in these calculations does not include the substituents on Tp that are present in the experimentally studied molecules. Steric hindrance from such groups may prevent the relaxation needed to stabilize the doublet. The tendency for the doublet to bend as predicted by NLSD is in full agreement with the Walsh diagram for TpCoI (Figure 7). The NLSD optimized quartet structure is essentially linear, i.e., the bending angle is predicted as $\alpha = 3.8°$, compared to $\alpha = 3.3°$ in the actual molecule. Table 4 lists comparative bond distances and angles; the agreement is very good. Figure 9c shows the calculated NLSD frontier orbital energy levels.

Summary. We have traced the electronic origins of the particular structures adopted by complexes of the type TpCo-L. Their geometries are determined by the nature of the ligand L and the d-electron count of the metal. The choice of ligand establishes the relative energies of the frontier molecular orbitals. In combination with the actual occupation of the frontier orbitals, the balance may be tipped toward either linear or bent structures. In particular, the combination of a ligand which is both a good σ-donor and π-acceptor (e.g., CO) and a d^8 electron count leads to a "bent" structure. Beyond the qualitative analysis, we have found that geometry optimization with DFT calculations yield structural parameters for these relatively large molecules that agree to high accuracy with X-ray structure determinations.

Experimental Section

Reagents and General Techniques. All manipulations involving air-sensitive organometallic compounds were carried out in a Vacuum Atmospheres inert atmosphere glovebox under nitrogen. All solvents were distilled under nitrogen from purple benzophenone ketyl. CoI_2 was obtained from the Strem Chemical Company. ^{1}H-NMR spectra were recorded on a Bruker AM 250 MHz spectrometer in C_6D_6 solvent, using residual C_6D_5H ($\delta = 7.15$ ppm) as a reference. Infrared spectra were recorded on a Mattson Instruments Alpha Centauri spectrometer. UV−visible spectra were obtained with a Bruins spectrophotometer. Magnetic susceptibilities were recorded on a Johnson Matthey magnetic susceptibility balance. Mass spectral data were performed by the University of Delaware Mass Spectrometry Facility. Elemental analyses

(38) Parr, R. G.; Yang, W. *Density Functional Theory of Atoms and Molecules*; Wiley: New York, 1986.
(39) Russo, T. V.; Martin, R. L.; Hay, P. J. *J. Chem. Phys.* **1994**, *101*, 7729.

were carried out by ORS laboratory services. X-ray crystallographic studies were performed by the University of Delaware X-ray crystallographic Facility.

Iodo-hydrotris(3-neopentylpyrazolyl)borato-cobalt (II), $Tp^{Np}CoI$. $Tp^{Np}Tl$ was prepared according to Trofimenko et al.[16] To a solution of 1.0 g of $Tp^{Np}Tl$ (1.60 mmol) in 250 mL of THF was added 0.500 g of CoI_2 (1.60 mmol). The blue solution was stirred overnight and then filtered through Celite, and the solvent was removed in vacuo. The blue residue was recrystallized from toluene: yield 0.600 g (61.6%); ^1H NMR (C_6D_6) 8.637 (27H), 12.30 (6H), 28.35 (3H), 75.45 (3H) ppm; IR (KBr) 2955 (s), 2905 (m), 2866 (m), 1508 (m), 1402 (m), 1362 (m), 1316 (w), 1279 (w), 1238 (w), 1186 (s), 1140 (m), 1051 (s), 791 (m), 768 (w), 706 (m), 675 (w) cm^{-1}; UV−vis (THF) 390 (ϵ = 428 M^{-1} cm^{-1}), 610 (ϵ = 686 M^{-1} cm^{-1}), 640 (ϵ = 886 M^{-1} cm^{-1}), 920 (ϵ = 143 M^{-1} cm^{-1}), 1725 (ϵ = 86 M^{-1} cm^{-1}) nm; mp 190−192 °C; μ_{eff} = 5.1(1) μ_B (295 K); MS (*m/e*) 482 (100%), 481 (26.8%), 440 amu (88%), 109 amu (31.1%), 82 amu (41.7%). Anal. Calcd for $C_{24}H_{40}BCoN_6I$: C, 47.29; H, 6.57; N, 13.79. Found: C, 47.39; H, 6.65; N, 13.79.

μ-Dinitrogen-bis(hydrotris(3-neopentylpyrazolyl)borato)-dicobalt (I), $[Tp^{Np}Co]_2(\mu\text{-}N_2)$. To a solution of 500 mg of $Tp^{Np}CoI$ (0.821 mmol) in THF was added an excess of Mg turnings. The solution was stirred until it had turned brown. It was filtered, and the solvent was removed in vacuo. The brown residue was recrystallized from pentane: yield 260 mg (64%); ^1H NMR (C_6D_6) −10.66 (6H), 0.60 (27H), 33.33 (3H), 48.14 (3H) ppm. IR (KBr): 2949 (s), 2903 (m), 2864 (m), 2056 (ν_{NN}, vw), 1507 (m), 1476 (w), 1398 (w), 1362 (m), 1190 (s), 1136 (w), 1096 (w), 1045 (s), 752 (w), 718 (w) cm^{-1}; UV−vis (THF) 783 (ϵ = 808 M^{-1} cm^{-1}), 992 (ϵ = 752 M^{-1} cm^{-1}), 1562 (ϵ = 484 M^{-1} cm^{-1}) nm; mp 161−163 °C; μ_{eff} = 4.1(1) μ_B per Co (295 K); MS (*m/e*) 482 (100%), 481 (26.8%), 440 (88%), 109 (31.1%). Anal. Calcd for $C_{48}H_{80}B_2Co_2N_{14}$: C, 58.07; H, 8.06; N, 19.75. Found: C, 58.00, H, 7.84, N, 19.56.

Carbonyl-hydrotris(3-neopentylpyrazolyl)borato-cobalt (I), Tp^{Np}-Co(CO). To a stirred solution of 400 mg of $[Tp^{Np}Co]_2(\mu\text{-}N_2)$ (0.403 mmol) in pentane in an ampule was added as excess of CO. A color change from brown to blue-green occurred immediately. The solution was filtered and concentrated for recrystallization: yield 411 mg (100%); ^1H NMR (C_6D_6) −14.10 (6H), −0.90 (27H), 31.60 (3H), 36.00 (3H) ppm; IR (KBr) 2951 (s), 2905 (m), 2864 (m), 1950 (w), 1508 (s), 1478 (w), 1398 (w), 1362 (m), 1262 (m), 1192 (m), 1098 (vs), 1049 (vs), 797 (m), 756 (w), 712 (w) cm^{-1}; UV−vis (THF) 656 (ϵ = 238 M^{-1} cm^{-1}), 1135 (ϵ = 274 M^{-1} cm^{-1}) nm; mp 122−124 °C; μ_{eff} = 3.1(1) μ_B (295 K); MS (*m/e*) 483 (100%), 482 (100%), 329 (93%), 273 (53%). Anal. Calcd for $C_{25}H_{40}BCoN_6O$: C, 58.82; H, 7.84; N, 16.47. Found: C, 58.37; H, 7.97; N, 16.24.

Tetrakis(tetrahydrofuran)magnesium Bis[carbonyl-hydrotris(3-*tert*-butyl-5-methyl-pyrazolyl)borato cobaltate (0)], $[Tp'Co(CO)]_2Mg(THF)_4$. To a stirred solution of 500 mg of Tp′Co(CO) in THF in an ampule was added excess Mg. The solution was stirred until it turned red. The solution was filtered and concentrated for recrystallization with excess Mg added to the solution: yield 658 mg (88.8%); ^1H NMR (C_6D_6) −24.85 (27 H), 7.80 (9H), 33.23 (3H) ppm; IR (Nujol) 2954 (s), 2928 (s), 2853 (s), 1642 (m), 1539 (w), 1452 (m), 1377 (w), 1192 (w), 1063 (w), 783 (w) cm^{-1}. Due to the extreme sensitivity of this complex further characterization was not attempted.

Crystal Structure Determination of $[(Tp^{neo}Co)_2(u\text{-}N_2)]$, Tp^{neo}-CoCO, and $(Tp'CoCO)_2Mg(THF)_4$. Single crystals of $[(Tp^{Np}Co)_2(\mu\text{-}N_2)]$, $Tp^{Np}Co(CO)$, and $[Tp^{t\text{-}Bu,Me}Co(\mu\text{-}CO)]_2Mg(THF)_4$ were sealed in glass capillaries under N_2. Lattice constants were determined by a least-squares fit of 15 diffractometer-measured 2 Θ values. The structures were solved by direct methods. Hydrogen atom parameters were generated from assumed geometries and were not refined. No absorption correction was applied. Full-matrix least-squares refinement was carried out with SHELXTL PLUS 4.2 on a 486 IBM computer. Crystals $[(Tp^{Np}Co)_2(\mu\text{-}N_2)]$ and $[Tp^{t\text{-}Bu,Me}Co(\mu\text{-}CO)]_2Mg(THF)_4$ diffracted weakly but represented the best specimens available after screening samples from several attempts to obtain better crystals. The high residuals are a common occurrence for bulky Tp complexes. Coordinates and thermal parameters are included in the supplementary material. See Table 5 for crystallographic data.

Theoretical Methods. The density functional calculations reported here are based on the Kohn and Sham approach to density functional theory (DFT),[40,41] later generalized by Levy.[42] Two different implementations of DFT were used, DMol[34] and DGauss.[35] Both programs incorporate the local spin density approximation (LSD) as well as a nonlocal correction to this approximation (NLSD).

DMol uses numerical basis sets which are given as tabulated values of multipolar functions. The calculation were performed with double numerical basis functions together with polarization functions (DNP). This basis set is comparable in size to Gaussian 6-31G** sets. The unrestricted Kohn−Sham (UKS) equations were solved self-consistently with the local spin density approximation (LSD) of Vosko−Wilk−Nusair.[43] A numerical grid of 3500 points per atom was used.

DGauss uses Gaussian orbitals as basis functions. Calculations were done with a double-ζ basis set with polarization functions (DZVP) and the A1 auxiliary basis sets for the density fitting. The UKS calculation were performed using the Vosko−Wilk−Nusair potential including Becke-Perdew gradient (nonlocal) corrections (NLSD).[44−46] Nonlocal corrections were added self-consistently.

The extended Hückel (EHT) calculations as well as construction of the Walsh diagrams were performed using the CACAO program.[47] The EHT based Walsh diagrams were constructed by using nine points on the reaction coordinate.

Acknowledgment. This research was supported by grants from DOE (ER14273 to K.H.T.) and from NSF (CHE-9401312 to D.J.D.). We also wish to thank Thomas Raeuchle and George Fitzgerald for their support and advice in use of DGauss and Cray Research Corporation for providing computer time.

Supporting Information Available: Tables giving the positional and thermal parameters of $[(Tp^{Np}Co)_2(\mu\text{-}N_2)]$, Tp^{Np}-Co(CO), and $[Tp^{t\text{-}Bu,Me}Co(\mu\text{-}CO)]_2Mg(THF)_4$ (16 pages). This material is contained in many libraries on microfiche, immediately follows this article in the microfilm version of the journal, can be ordered from the ACS, and can be downloaded from the Internet: see any current masthead page for ordering information and Internet access instructions.

JA9523101

(40) Hohenberg, P.; Kohn, W. *Phys. Rev. B* **1964**, *136*, 864.
(41) Kohn, W.; Sham, L. *J. Phys. Rev. A* **1965**, *140*, 1133.
(42) Levy, M. *Proc. Natl. Acad. Sci. U.S.A.* **1979**, *76*, 6062.
(43) Vosko, S. H.; Wilk, L.; Nusair, M. *Can. J. Phys.* **1980**, *58*, 1200.
(44) Becke, A. D. *Phys. Rev. A.* **1988**, *38*, 3098.
(45) Becke, A. D. *ACS Symp. Ser.* **1989**, *394*, 165.
(46) Perdew, J. P. *Phys. Rev. B* **1986**, *33*, 8822.
(47) Mealli, C.; Proserpio, D. M. *J. Chem. Edu.* **1990**, *67*, 399.